
DÉPARTEMENT DE MICROTECHNIQUE
INSTITUT DE SYSTÈMES ROBOTIQUES
AUTONOMOUS SYSTEMS LABORATORY



Windball

Moritz v. Heimendahl
Département de Physique

October 26, 2004

Assistants: Thomas Estier
Pierre Lamon
Professor: Roland Siegwart

Contents

1	Introduction	3
1.1	Motivation	3
1.2	Goals	3
1.3	Methodology	4
2	Theoretical background	5
2.1	Martian environment	5
2.1.1	General properties	5
2.1.2	Temperature variations	6
2.1.3	Winds	6
2.1.4	Surface properties	6
2.2	Aerodynamics	6
2.2.1	Laminar and turbulent flow	6
2.2.2	The Reynolds number	6
2.2.3	Drag force of a sphere	8
2.2.4	Boundary layers	8
2.3	Similarity laws	9
2.3.1	Kinematic similarity	10
2.3.2	Dynamic similarity	11
2.3.3	Reynolds similarity	12
2.4	Shape memory alloys	13
2.4.1	Definition and characteristics	13
2.4.2	Application	14
2.4.3	Comparison to bimetallic components	16
3	Robot design	17
3.1	The Windball concept	17
3.2	Application scenario	17
3.3	Two variants	18
3.4	Weight	20
3.4.1	Hardball	20
3.4.2	Softball	20
3.5	Mobility performance	21
3.5.1	Maximum step height	21
3.5.2	Mean free path	24
3.5.3	Model limits	28
3.5.4	Model evaluation	28

4	Experiments	30
4.1	Movitation	30
4.2	Aims	30
4.3	Setup	30
4.4	Observations	31
4.5	Interpretation	32
5	Conclusion & Outlook	34
5.1	Summary of results	34
5.1.1	Hardball vs. Softball	34
5.1.2	Evaluation of the methodology	34
5.2	Assessment of feasibility	34
5.2.1	Realization	34
5.2.2	More data	35
5.3	Necessary future development	35
5.3.1	Model refinement	35
5.3.2	Experiments	35
5.3.3	Overall design	35
5.3.4	Environment and landing site	35
	Acknowledgements	36
	Bibliography	37

Chapter 1

Introduction

1.1 Motivation

The acquisition of more ground data from Mars would be desirable for Mars research in general, but especially for projects like the search for traces of life. During previous landing missions, lacking mobility of the lander has been limiting the possibilities to gather data from the Martian surface.

NASA's Pathfinder mission was a step ahead in that sense, with a rover exploring the surroundings of the landing site. However, while being a success in its own right, it clearly showed the main problems that limited the rover's range: insufficient energy supply and difficulties to communicate with the lander [NA1]. They are aggravated by the tough Martian environment: Wind and dust make the use of solar cells difficult [Lan98], high temperature differences decrease the efficiency of chemical batteries and rocks lying around complicate the task to navigate.

A new approach might prove worthy: Instead of trying to adapt an existing robot design to the Martian conditions, one could try to develop a new robot concept that integrates the characteristics of the target environment from the beginning; that, instead of suffering from these unfavourable conditions, exploits them wherever possible.

1.2 Goals

The goal of my semester project was to examine the feasibility of a robot as sketched above. The design that has been proposed, covered in detail in chapter 3, describes a robot of spherical form that is driven by the wind. Therefore, we mainly focused on the aerodynamics of the robot. In particular, we tried to answer two questions: Is the wind strong enough to move the robot around in a rocky Martian landscape; and which design parameters yield the best mobility performance?

1.3 Methodology

In order to study the robot's aerodynamics, two methods were combined: Theoretical modelling and experiments. This required the knowledge of the Martian environment as well as certain basics in fluid dynamics. As the experiments were made at a reduced scale in an environment different from the Martian one, similarity laws had to be respected, too. Finally, the robot's design may include the use of shape memory alloys, so that all these theoretical topics will have to be covered in chapter 2.

What follows is the presentation of the robot concept and the description of the model to evaluate the robot's mobility (chapter 3). This model being very simplistic, its results are compared to the evidence of an experiment (chapter 4).

Based on all the evidence gathered, we will finally assess the general feasibility of the project and indicate the next steps to take (chapter 5).

Chapter 2

Theoretical background

2.1 Martian environment

2.1.1 General properties

“*Mars is red and small and cold*” says a NASA website [NA2]. Quantitatively, Table 2.1 gives a synopsis of some properties of our closest neighbour. More data can be found in [Mor96], [NA3] and [Col96].

mean distance from sun	227,940,000 km
orbital eccentricity	0.0934
tilt of axis	25.19°
duration of a day	24.6 h
duration of a year	687 earth days
diameter	6787 km
mass	$6.42 \cdot 10^{23}$ kg
gravity constant	$3.73 \frac{\text{m}}{\text{s}^2}$
mean temperature	-53 °C
typical diurnal temperature variation	30...100 °C
surface atmospheric pressure	6...10 hPa
average wind speed	$\approx 7 \frac{\text{m}}{\text{s}}$
main atmosphere component	CO ₂

Table 2.1: General properties of Mars

Mars is about 50% farther from the sun than earth, and the orbit is a lot more eccentric. This, taken together with the axis tilt, results in asymmetric seasons: The southern summer is a lot hotter than the northern one, provoking the famous sand storms (see section 2.1.3). As can be seen, Mars has a similar day-and-night rhythm to earth. Its smaller size and mass result in a gravity constant which is about $\frac{1}{3}$ of that of earth. It is generally cold on Mars, and the temperature variations between day and night are very high due to the lack of water and the thin atmosphere: The surface pressure is about 150 times lower than on earth.

2.1.2 Temperature variations

Figure 2.1 shows daily temperature variations on Mars, for different latitudes and weather conditions. Around the equator, we can observe daily surface temperature variations between 100°C (clear atmosphere) and 60°C (dusty atmosphere).

Figure 2.2 displays the evolution of this daily cycle through the year; in a belt from roughly 30°N to 30°S the minima are always below -70°C and the maxima above -20°C . The poles, especially during winter, have weaker variations.

2.1.3 Winds

While the average wind speed was given as 7m/s , stronger winds are quite common: Great sand storms that may cover a whole hemisphere often occur during southern summer. Local dust storms, covering some $1\,000\,000\text{ km}^2$, are even more common, producing near-ground wind speeds of 50m/s and more [NA2], [Col96].

2.1.4 Surface properties

Mars is famous for its canals, and craters are common, too. However, there are regions that are relatively flat [NA4]. So, the choice of an appropriate landing site is essential for the success or failure of a Martian space mission. Consequently, an in-depth study of the Martian geography will be necessary later on.

2.2 Aerodynamics

For a thorough treatment of this subject, see [Ryh91].

2.2.1 Laminar and turbulent flow

In fluid dynamics, one generally distinguishes between laminar and turbulent flow. The latter is characterised by an erratic behaviour of the speed vector as a function of time at any given point. It is impossible to predict the path that a particle will follow from its starting point.

Laminar flow, however, is completely regular and deterministic, with neatly separated streamlines that indicate the particles' trajectories.

As one may expect, there is not just the one or the other, but a whole range of flow patterns that may be called more or less laminar or turbulent. In order to classify them, the so-called *Reynolds number*, noted Re , is introduced.

2.2.2 The Reynolds number

The Reynolds number may be considered a measure of turbulence: The higher it is, the more turbulent is the flow. In order to calculate the Re of any given system, one has to choose a reference length d – typically the size of an object in a flow – and a reference speed u , normally the relative velocity of the flow with

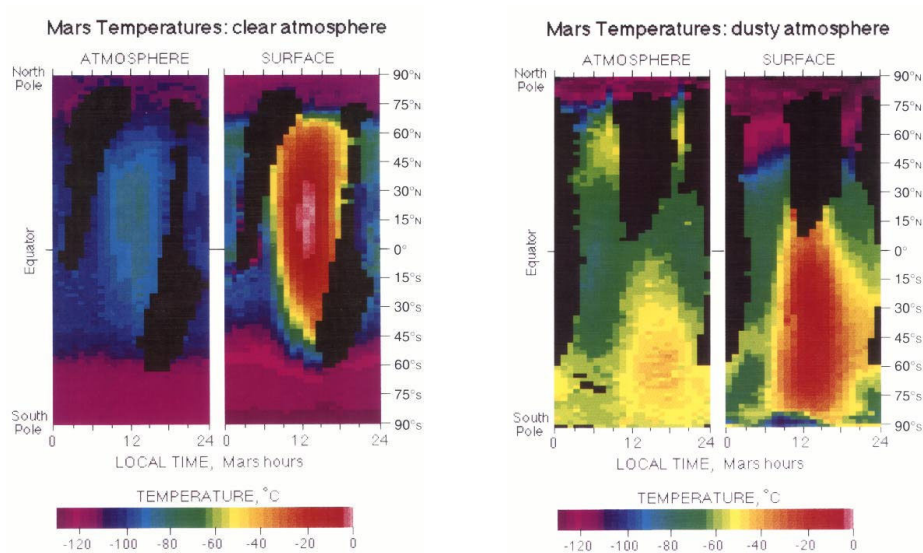


Figure 2.1: Temperature evolution during a Martian day as a function of latitude; black fields mean no data available [MST]

SEASONAL TEMPERATURE BEHAVIOR OF MARS

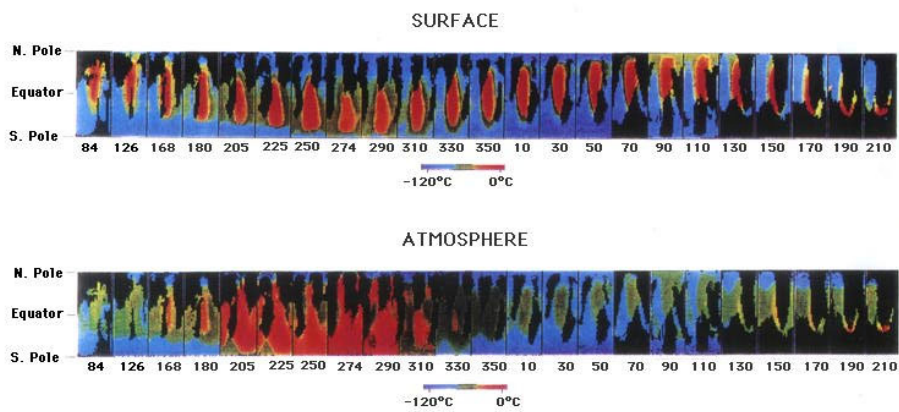


Figure 2.2: Temperature evolution for different seasons [MST]

respect to the object. Then Re is calculated as

$$Re = \frac{u \cdot d}{\nu} \quad (2.1)$$

with ν the kinematic viscosity. It is related to the dynamic viscosity η by

$$\nu = \frac{\eta}{\rho} \quad (2.2)$$

with ρ being the density.

Thus, with Re 's definition varying from system to system, one cannot give a general, precise rule of a laminar or a turbulent range of Reynolds numbers. All we can say is the following:

If two systems are geometrically similar and have the same Re , then their flow patterns will be the same, too.

Consider, as an example, the case of a sphere in a linear, steady flow. From (2.1) we see that, the faster the flow, the higher Re and thus the more turbulent the flow. That may not be surprising. However, one might expect the flow to remain the same if the flow's speed and the sphere's size are rescaled by the same factor. Alas, this is not the case, because Re changes, and so does the flow's character.

The implications on scaling will be treated in detail in section 2.3.

2.2.3 Drag force of a sphere

Any object placed in a flow is acted upon by a certain drag force. For simple forms it is usually expressed as

$$F_d = c_d \cdot A \cdot \frac{1}{2} \rho v^2 \quad (2.3)$$

with c_d being the drag coefficient, A the area of the object's projection on a plane perpendicular to the flow, and ρ and v the density and speed of the flow, respectively. The coefficient c_d depends on the object's form and strongly on the Reynolds number. Figure 2.3 shows this dependence for some chosen geometries. Examining the graph marked "Kugel" (=sphere), we can distinguish several different regions corresponding to different flow phenomena:

For $Re < 1$, the flow is laminar and may be calculated analytically. c_d is proportional to Re^{-1} , so that the drag force is proportional to the flow speed.

For higher Re , the flow becomes more and more turbulent, and c_d has to be measured experimentally. For $1 > Re > 10^5$, c_d stabilises at ≈ 0.3 and F_d begins to rise with the square of the speed.

Then, between 10^5 and 10^6 , the flow pattern changes abruptly. In a narrow range of Re , the drag force actually *decreases* with rising speeds.

Summarising: If, for a given system, the dependence of c_d on Re is known, then (2.3) is a simple and useful formula. However, its applicability is restricted in the sense that it assumes a steady, homogenous flow.

2.2.4 Boundary layers

In the last section, we were considering a homogenous flow. In reality, this is a thing rarely to be found.

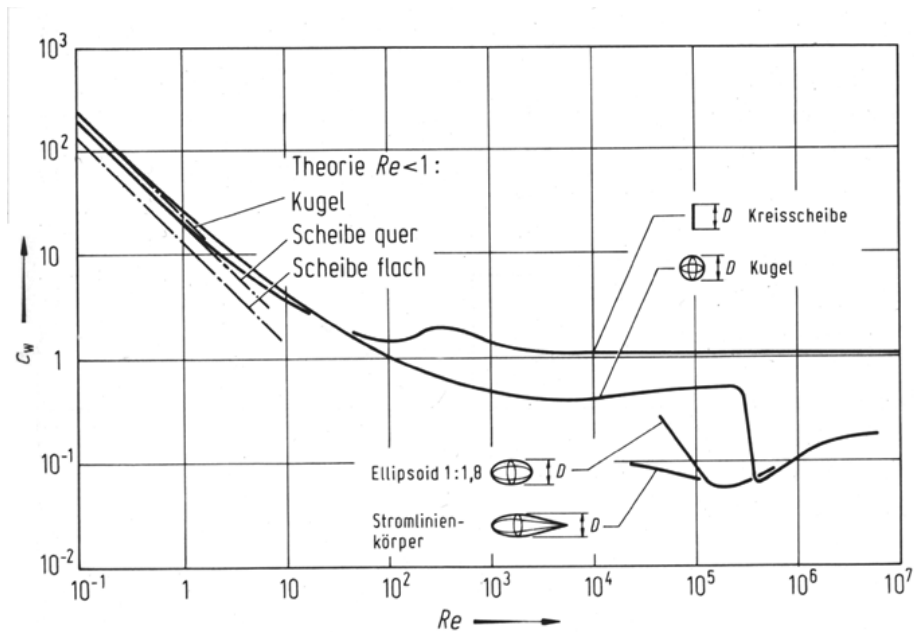


Figure 2.3: c_d as a function of Re for various geometries; the graph marked “Kugel” corresponds to a sphere [Ryh91]

Consider a flow that is delimited in one direction by a plane parallel to the flow. At zero distance from the surface, the flow velocity vanishes due to the viscosity of the fluid. Far from the surface, let the flow be almost homogenous and laminar. The domain that links those two regions is called the boundary layer. It is characterised by a non-negligible velocity gradient. Figure 2.4 gives an example of a velocity profile that may be found in a boundary layer.

However, the exact velocity distribution in a boundary layer depends on various parameters, as for example the Reynolds number that takes into account the asperity of the surface.

2.3 Similarity laws

For a general treatment, see [Her95].

Whenever a system is studied by way of scaled breadboard experiments, the model is supposed to reproduce the original as exactly as possible. How and to what extent this is possible is described by the similarity laws.

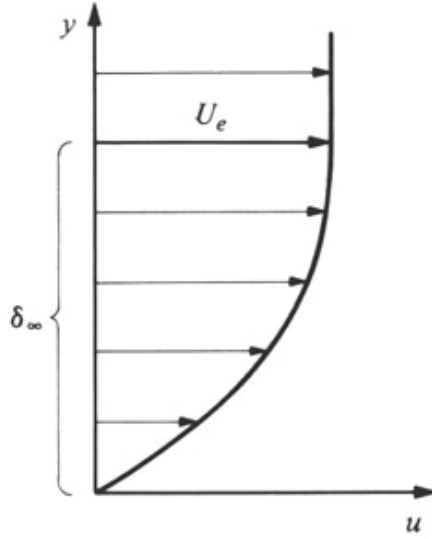


Figure 2.4: Typical velocity profile in a boundary layer; U_e is the velocity of the undisturbed flow, δ the thickness of the boundary layer [Ryh91]

2.3.1 Kinematic similarity

If we would like to reproduce movements, we have to consider the two kinematic equations

$$v = \frac{dx}{dt} \quad (2.4)$$

and

$$a = \frac{d^2x}{dt^2} \quad (2.5)$$

If we introduce non-dimensional variables as follows

$$x^* := \frac{x}{x_0}, t^* := \frac{t}{t_0}, v^* := \frac{v}{v_0}, a^* := \frac{a}{a_0} \quad (2.6)$$

then (2.4) and (2.5) become

$$v^* = \frac{x_0}{v_0 t_0} \frac{dx^*}{dt^*} \quad (2.7)$$

and

$$a^* = \frac{x_0}{a_0 t_0^2} \frac{d^2x^*}{dt^{*2}} \quad (2.8)$$

For a model to truly reproduce the movements of the original, each of the two factors

$$\frac{x_0}{v_0 t_0} \quad (2.9)$$

and

$$\frac{x_0}{a_0 t_0^2} \quad (2.10)$$

must be the same in both cases. This makes the equations describing the movement be the same.

The following definitions are commonly introduced:

$$\Pi_1 = \frac{x_0}{v_0 t_0} \quad (2.11)$$

and

$$\Pi_2 = \frac{x_0}{a_0 t_0^2} \cdot \Pi_1^2 = \frac{v_0^2}{x_0 a_0} \quad (2.12)$$

A priori, one is free to choose the scales for the four variables, as long as Π_1 and Π_2 remain the same. Yet, for systems that are influenced by gravity, the acceleration scale is fixed by the gravity constant g . If a_0 in Π_2 is replaced by g , then Π_2 becomes the so-called Froude number

$$Fr = \frac{v_0^2}{g x_0} \quad (2.13)$$

For Π_1 and Fr to remain constant, one is left with one single degree of freedom to choose the scale of the model. If we denote x_m and x_r the model's and reality's reference size, respectively, and likewise for the other variables, we get:

$$Fr_m = Fr_r \quad (2.14)$$

$$\frac{v_m^2}{g_m x_m} = \frac{v_r^2}{g_r x_r} \quad (2.15)$$

$$\boxed{\frac{v_m}{v_r} = \sqrt{\frac{g_m x_m}{g_r x_r}}} \quad (2.16)$$

The time scale will be fixed by the condition that

$$\Pi_{1m} = \Pi_{1r} \quad (2.17)$$

and we obtain

$$\boxed{\frac{t_m}{t_r} = \sqrt{\frac{x_m g_r}{x_r g_m}}} \quad (2.18)$$

2.3.2 Dynamic similarity

If we want dynamic similarity, we have to consider the forces that are acting. In particular, the ratios of the different forces must remain the same.

The special case that will be treated here is the behaviour of a sphere submitted to wind force and gravitation. The ratio between these two forces is, using (2.3)

$$\frac{F_w}{F_g} = \frac{c_d \cdot A \cdot \frac{1}{2} \rho v^2}{m g} \quad (2.19)$$

Using the same subscripts as in section 2.3.1, similarity is expressed by

$$\frac{c_d \cdot A_m \cdot \frac{1}{2} \rho_m v_m^2}{m_m g_m} = \frac{c_d \cdot A_r \cdot \frac{1}{2} \rho_r v_r^2}{m_r g_r} \quad (2.20)$$

The drag coefficient c_d is the same if the geometry and Re do not change (see section 2.3.3 for details). Using

$$A = x^2 \quad (2.21)$$

we find

$$\frac{m_m}{m_r} = \frac{x_m^2}{x_r^2} \frac{v_m^2}{v_r^2} \frac{\rho_m}{\rho_r} \frac{g_r}{g_m} \quad (2.22)$$

By substituting v by the expression given by (2.16), we get

$$\boxed{\frac{m_m}{m_r} = \frac{x_m^3}{x_r^3} \frac{\rho_m}{\rho_r}} \quad (2.23)$$

Summarising: By fixing the size of the model, and given the gravity constants and fluid densities for original and model, we automatically obtain the speed, time and mass scale for the model by equations (2.16), (2.18) and (2.23). So, we have only one degree of freedom to chose our scale.

2.3.3 Reynolds similarity

As explained in section 2.2.2, two flow patterns are similar if their Re are the same. Recalling definition (2.1):

$$Re = \frac{u \cdot d}{\nu} \quad (2.24)$$

and demanding

$$Re_m = Re_r \quad (2.25)$$

we get

$$\frac{u_m \cdot d_m}{\nu_m} = \frac{u_r \cdot d_r}{\nu_r} \quad (2.26)$$

Replacing for the speeds' ratio u_m/u_r the expression found in (2.16), we get

$$\frac{d_m}{d_r} = \left(\frac{g_r}{g_m} \right)^{1/3} \left(\frac{\nu_m}{\nu_r} \right)^{2/3} \quad (2.27)$$

which means that, if we cannot freely choose ν_m , we do not have any choice in picking the size scale!

So, we must verify if a differing Re implies strongly differing flow and forces, that is, if modelling with a different Re can still be meaningful. Experience shows that, as Re reaches high values, drag forces tend to vary less then for low values (see figure 2.3).

Moreover, a theory presented in [Her95] states that, as the flow gets very turbulent, its similarity is better expressed by conditions (2.16), (2.18) and (2.23) than by matching Reynolds numbers.

All this does not mean we can simply neglect the Reynolds factor. In section 2.2.3, we mentioned the drastic change of c_d at Re values between 10^5 and 10^6 . The moral is: working with Reynolds numbers different from those of the original requires careful study of the aerodynamic behaviour.

easier to deform. This is indicated by the curve from (C) to (D), which is less steep than from (A) to (B). Moreover, after releasing at (D), the solid does *not* return to (C), but will remain deformed (E). Only upon heating will happen what gave the SMAs their name: It will regain its original form (A).

The temperature range in which the transformation takes place typically extends over some 20-40°C. The absolute temperatures depend strongly on the elements used. For NiTi, a widely used SMA, the critical temperature A_f (see figure 2.5) is about +100°C for the equiatomic alloy, but can be lowered down to -200°C by addition of excess Ni.

2.4.2 Application

The fact that temperature changes may induce shape changes in SMAs soon made people think about temperature-activated components. Unfortunately, SMAs work only in one way²: In figure 2.5 we can go from (E) to (A) by heating, but not back to (E) simply by cooling. In order to return to the deformed state (E), some external force is needed.

Figure 2.6 shows a possible way to build a two-component system that solves this problem: A shape memory coil is combined with a generic coil spring,

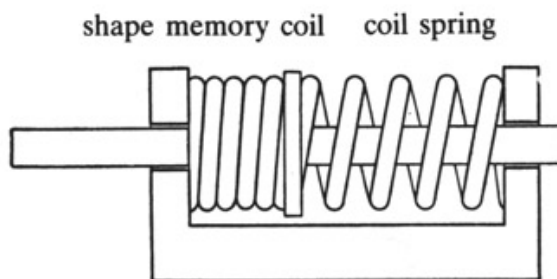


Figure 2.6: Two-way shape memory component [Fun84]

considered unsusceptable to temperature changes.

Figure 2.7 illustrates the behaviour of the system: on the x-axis the position of the centrepiece is marked, and on the y-axis the pulling force of each coil. Thus, if no other external forces are present, the equilibrium position is defined by the intersection of the two coils' graphs. Two extreme cases are shown: for high temperatures, the SMA coil is in its austenitic state and contracted; the equilibrium position is left of the centre (A). For low temperatures, the martensitic SMA is easier to deform, shifting the equilibrium towards the coil spring (B).

Unfortunately, things look less favourable if we introduce a force that is opposed to the movement of the system. Now the equilibrium is reached when the difference between the coils' forces equals that external force. Figure 2.7 shows clearly the subsequent reduction of the effective displacement from (A)–(B) to (A')–(B') under the effect of a 0.5N force.

²By sophisticated methods, it is possible to make SMAs change shape in both ways, but this technology still poses various problems.

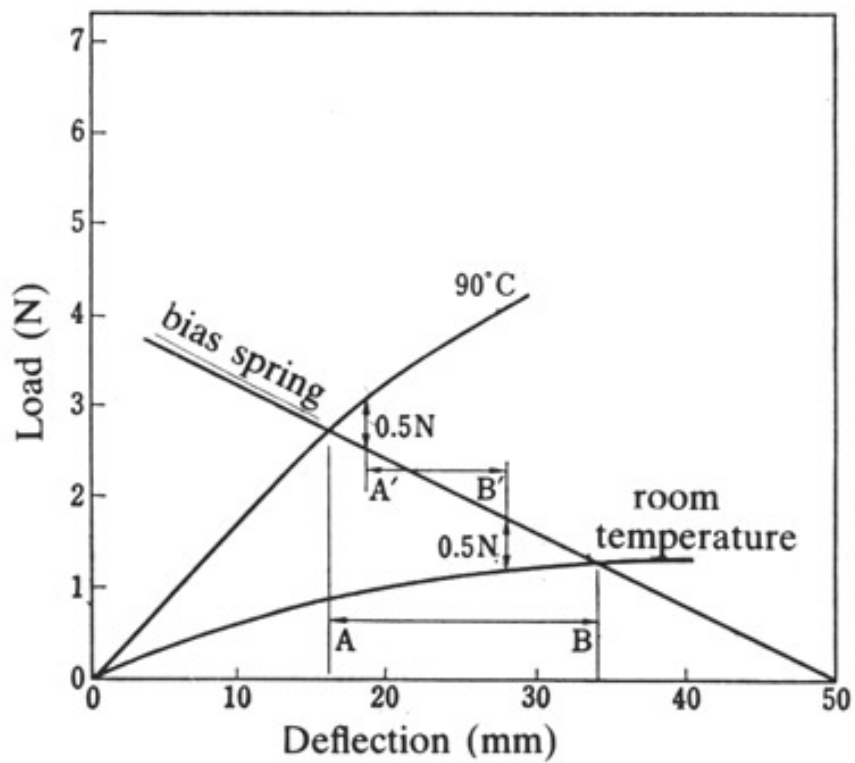


Figure 2.7: Force equilibria in the two-way shape memory component: the graph marked “bias” corresponds to the spring coil, the graphs “90°C” and “room temperature” are the SMA in its austenitic and its martensitic state, respectively [Fun84]

2.4.3 Comparison to bimetallic components

Bimetallic strips are a well-known and easy-to-handle alternative to SMAs as temperature-activated components. However, to give an example for their performance: The strains reached for temperature differences of 80°C with bimetallic strips are lower by a factor of $\approx 5\text{...}10$ with respect to SMAs (see figure 2.8).

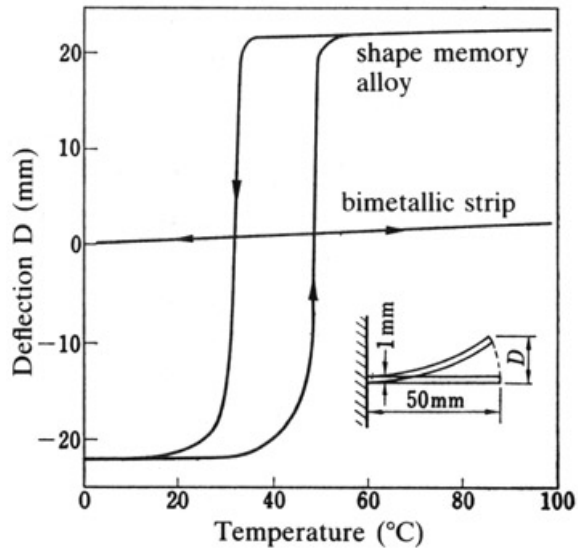


Figure 2.8: Bimetall vs. SMA [Fun84]

Chapter 3

Robot design

3.1 The Windball concept

As stated in the introduction, we wanted to conceive a robot that exploits the environmental conditions found on Mars. We came up with the following idea:

The robot has a form with axial symmetry (e.g. a cylinder or a sphere), which allows it to roll as a whole; the driving force is the Martian wind, which gave it the name “Windball”. It needs to be able to stop in order to produce energy, be localised by an orbiter and take measures. This is achieved by some change in shape which inhibits rolling. The deformation may be accomplished by the use of shape memory alloys: In the equatorial belt of Mars the daily temperature variations are always greater than 50° (see section 2.1.2), so that a judiciously chosen SMA (for example Ni-doped NiTi, see section 2.4) will perform a whole transformation cycle per day.

In this way, the two problems presented in section 1.1, that is energy supply and communication, would be solved in an elegant way: the energy needs are covered by exploiting inexhaustible resources of the Martian environment, and the need to communicate is drastically reduced without the need to navigate actively.

On the other hand, of course, this means that we have no active control of where the robot will go. But, with almost the whole surface of Mars left to discover, that need not be a great disadvantage.

3.2 Application scenario

The Windball would essentially work in two different modes: A displacement mode, with maximised wind resistance, during which there is neither control nor communication; and a resting mode, during which the robot measures some physical property, be it geological, meteorological or other, of the place where it is situated. In resting mode, it would, too, take contact with an orbiter, thus allowing to know its position on the planet, and generate the energy to feed the analysis and communication devices.

If shape memory alloys are used for the shape change, they would fulfil one deformation cycle per day, in accordance with the temperature change. So, the Windball could be in displacement mode at night and in resting mode at day.

If we would like to use solar cells to produce energy, it is, of course, preferable to move at night and rest during the day, and not vice versa (see figure 3.1).

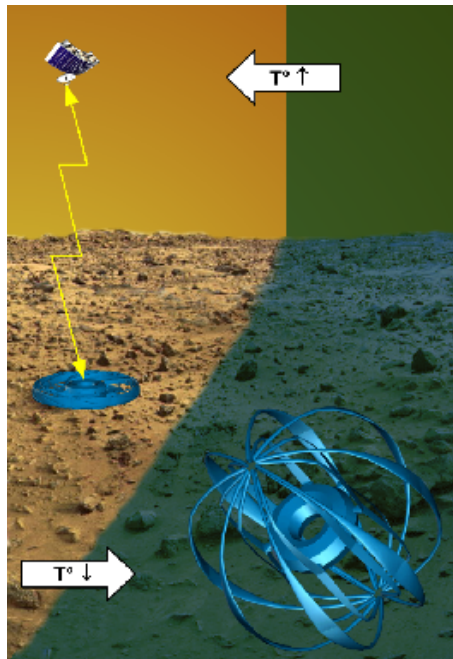


Figure 3.1: Application scenario for the Windball

3.3 Two variants

Two different versions of the Windball were considered:

According to the original idea it has a spherical, open, metallic structure (see figure 3.2 for one possible realisation) with a payload at its centre. The diameter would be in the range of one meter. The shape change, achieved by SMA actuators, transforms it into some flat, disk-like form, bringing the payload to the ground.

In the second version, (see figure 3.3) which is due to an idea of Prof. P. Monkewitz, the Windball is an inflatable balloon and of much bigger size; some 5 to 20 meters are planned. The deformation might be accomplished or by SMA actuators or by partially deflating the balloon.

To distinguish the two variants, the first one will be called “Hardball” and the second one “Softball”.

The motivations for the Softball are the problems of the Hardball: An open structure is likely to get stuck with some obstacle that has a size similar to the robot’s open spaces. Moreover, the Hardball might be too heavy to be moved by the wind.

On the other hand, the Softball’s enormous size is a drawback when it has to be carried to Mars, and the application of solar cells could be more difficult.

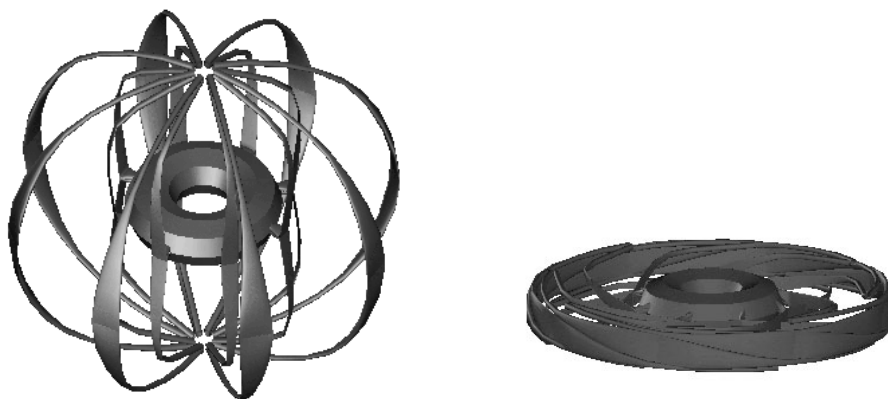


Figure 3.2: First Windball version: the Hardball; displacement mode (left) and resting mode (right)

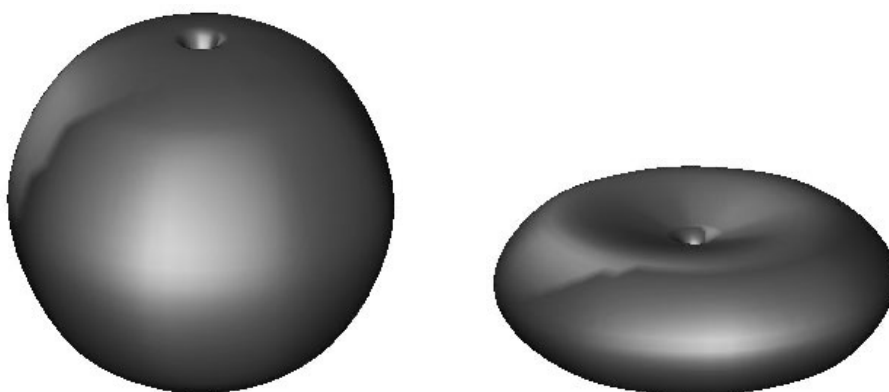


Figure 3.3: Second Windball version: the Softball; displacement mode (left) and resting mode (right)

3.4 Weight

3.4.1 Hardball

For the Hardball, dead reckoning let us assume a weight of the structure of 1kg for a diameter of 1m, plus 100g for the payload. But, what is more important: The mass will rise with at least the cube of the diameter, because the structure is three-dimensional.

3.4.2 Softball

The Softball's mass, however, grows as the square of the diameter. The following consideration will prove this.

The tension in a balloon's skin is [Hal01]

$$\sigma = \frac{p \cdot R}{d} \quad (3.1)$$

with σ the tension, R the radius of the balloon, p the pressure inside and d the skin's thickness. Thus, for a given material with a certain tensile strength σ_t , the minimum thickness is

$$d \geq \frac{p \cdot R}{\sigma_t} \quad (3.2)$$

Let us consider the balloon fully inflated when it rests on a circle whose radius is a fraction α of the balloon's radius. The inside pressure integrated over this area must sustain the balloons weight:

$$p \cdot \pi(\alpha R)^2 = m \cdot g \quad (3.3)$$

The mass m (neglecting the payload) is

$$m = 4\pi R^2 d \cdot \rho \quad (3.4)$$

with ρ the skin material's density. Inserting (3.4) into (3.3) and solving for p yields

$$p = \frac{4\pi R^2 d \cdot \rho \cdot g}{(\alpha R)^2 \pi} = 4\alpha^{-2} d \rho g \quad (3.5)$$

Replacing this for p in (3.2), we finally get

$$d \geq d \cdot \frac{4R\rho g}{\alpha^2 \sigma_t} \quad (3.6)$$

and d cancels out! We get a general condition that limits the size in terms of the skin material's tensile strength and the degree of inflation α :

$$R \leq \frac{\alpha^2 \cdot \sigma_t}{4\rho g} \quad (3.7)$$

But: d does **not** depend on R . The minimum d will be given by fabrication limits or other parameters, but it does not grow with the general scale of the Softball. So, its mass (neglecting the gas inside) will be proportional to its surface, i.e. to R^2 .

We guessed $d = 0.1\text{mm}$ to be a sufficient skin thickness for a material like Kevlar. With $R = 5\text{m}$, that would make a mass of $m = 45\text{kg}$.

3.5 Mobility performance

In order to evaluate the mobility of the Windball on Mars, we developed a two-layer model: At first, using purely physical considerations, we calculated the maximum height of a step that the robot would be able to climb. Then, we used statistical data of the rock size distribution on Mars to estimate the mean free path the Windball could make before hitting a boulder too big to climb over. All this was calculated as a function of wind speed, the robot's size and its mass. So, we can compare the two Windball variants and take a guess for each one's optimal size.

3.5.1 Maximum step height

The scenario is the following: We imagine the Windball to have come to a rest in front of a boulder, symbolised by a perfect step (see figure 3.4). In order to

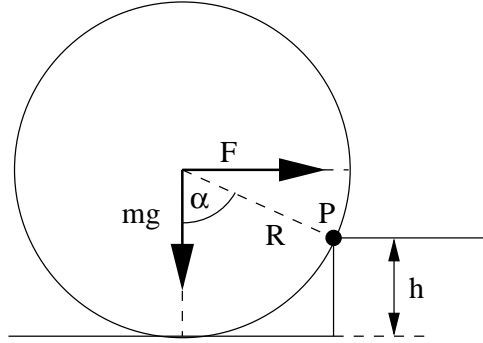


Figure 3.4: Windball blocked by a boulder

climb the step, the ball must turn about the point P . So, we must consider the net torque with respect to P . The two forces acting are gravity (marked mg) and the wind force F . Taking into account their lever arms, we must have

$$F \cdot \cos \alpha > mg \cdot \sin \alpha \quad (3.8)$$

$$\Rightarrow \frac{F}{mg} > \tan \alpha \quad (3.9)$$

Expressing α in terms of the step height h and the sphere's radius R

$$\cos \alpha = \frac{R - h}{R} \quad (3.10)$$

we get

$$\frac{R - h}{R} > \cos \left(\arctan \frac{F}{mg} \right) \quad (3.11)$$

and solving for h

$$h < R \cdot \left(1 - \cos \left(\arctan \frac{F}{mg} \right) \right) \quad (3.12)$$

To find the forward force F , we consider the flow to be approximately uniform. That allows us to use (2.3) to find the force acting on the Windball. A c_d of 0.3 was used for the Softball, which is the value for a sphere at high Re .

For the Hardball, however, we assumed $c_d = 1.1$, the value for a disk perpendicular to the flow, to take into account the open design structure. That may appear little reasonable, or even as wishful thinking, but, as a matter of fact, the c_d of an irregular structure composed of intersecting plates or disks (even with openings) may be higher than that of a smooth sphere. That may seem counterintuitive, but intuition is a bad method to approach aerodynamics; an example for this is the fact that the c_d of a disk *rises* when a small hole is cut into it (see Hoerner [Hoe51] for a complete treatment of the drag force). Still, using a c_d of 1.1 for the Hardball may be considered optimistic and has to be verified by experiments.

Tables 3.1 and 3.2 show the maximum step heights for the Hardball and the Softball, respectively. Figures 3.5 and 3.6 show graphs of the same data.

mass /kg	radius /m	wind speed / $\frac{m}{s}$								
		3	6	9	12	15	18	22	26	30
0.127	0.15	1.36E-05	2.17E-04	1.09E-03	3.37E-03	7.85E-03	1.50E-02	2.85E-02	4.46E-02	6.06E-02
0.164	0.2	3.44E-05	5.49E-04	2.73E-03	8.27E-03	1.86E-02	3.37E-02	5.84E-02	8.34E-02	1.05E-01
0.316	0.3	7.04E-05	1.12E-03	5.55E-03	1.65E-02	3.62E-02	6.34E-02	1.05E-01	1.43E-01	1.74E-01
1.10	0.5	7.47E-05	1.19E-03	5.95E-03	1.81E-02	4.10E-02	7.55E-02	1.34E-01	1.95E-01	2.50E-01
4.20	0.8	5.38E-05	8.60E-04	4.33E-03	1.34E-02	3.17E-02	6.18E-02	1.21E-01	1.97E-01	2.78E-01
8.10	1	4.41E-05	7.05E-04	3.55E-03	1.11E-02	2.65E-02	5.27E-02	1.07E-01	1.83E-01	2.71E-01
13.9	1.2	3.71E-05	5.94E-04	3.00E-03	9.40E-03	2.26E-02	4.54E-02	9.48E-02	1.67E-01	2.57E-01
27.1	1.5	2.99E-05	4.78E-04	2.42E-03	7.60E-03	1.84E-02	3.73E-02	7.97E-02	1.45E-01	2.32E-01
64.1	2	2.25E-05	3.60E-04	1.82E-03	5.74E-03	1.39E-02	2.86E-02	6.22E-02	1.16E-01	1.93E-01

Table 3.1: Hardball max step height

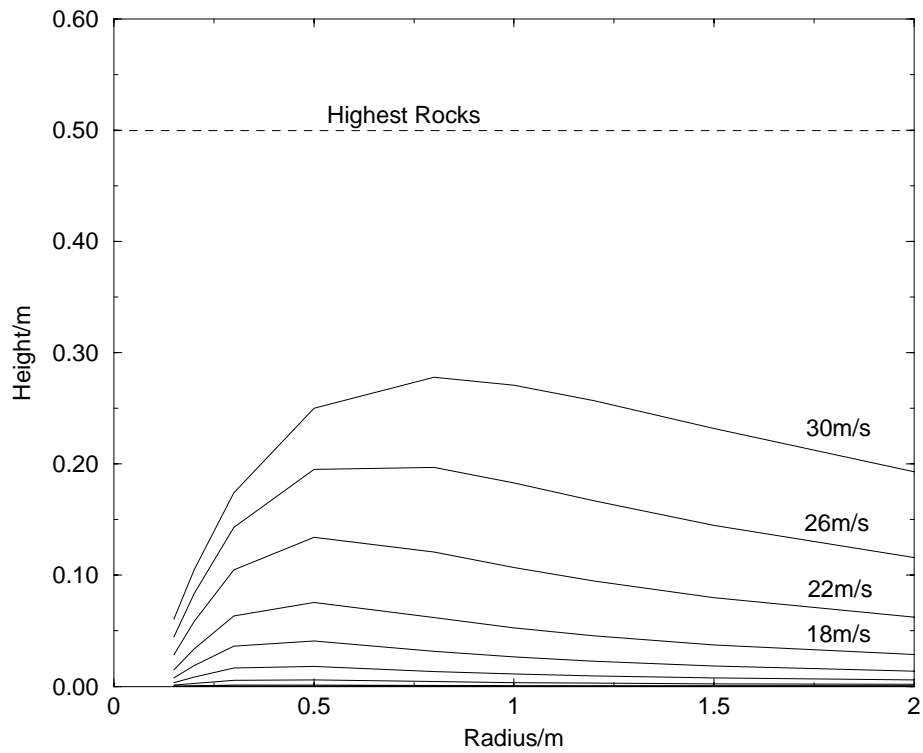


Figure 3.5: Hardball maximum step height

mass /kg	radius /m	wind speed/ $\frac{m}{s}$								
		3	6	9	12	15	18	22	26	30
1.91	1	5.90E-05	9.43E-04	4.74E-03	1.48E-02	3.50E-02	6.87E-02	1.37E-01	2.25E-01	3.23E-01
7.34	2	1.28E-04	2.04E-03	1.03E-02	3.19E-02	7.54E-02	1.48E-01	2.91E-01	4.76E-01	6.75E-01
16.39	3	1.95E-04	3.11E-03	1.56E-02	4.86E-02	1.15E-01	2.24E-01	4.42E-01	7.21E-01	1.02E+00
45.35	5	3.27E-04	5.22E-03	2.63E-02	8.17E-02	1.93E-01	3.77E-01	7.41E-01	1.21E+00	1.71E+00
181.1	10	6.56E-04	1.05E-02	5.27E-02	1.64E-01	3.87E-01	7.55E-01	1.49E+00	2.42E+00	3.42E+00
260.7	12	7.88E-04	1.26E-02	6.33E-02	1.97E-01	4.64E-01	9.07E-01	1.78E+00	2.90E+00	4.11E+00
407.4	15	9.85E-04	1.57E-02	7.91E-02	2.46E-01	5.80E-01	1.13E+00	2.23E+00	3.63E+00	5.14E+00
523.2	17	1.12E-03	1.78E-02	8.97E-02	2.79E-01	6.58E-01	1.28E+00	2.53E+00	4.12E+00	5.82E+00
724.1	20	1.31E-03	2.10E-02	1.06E-01	3.28E-01	7.74E-01	1.51E+00	2.97E+00	4.84E+00	6.85E+00

Table 3.2: Softball max step height

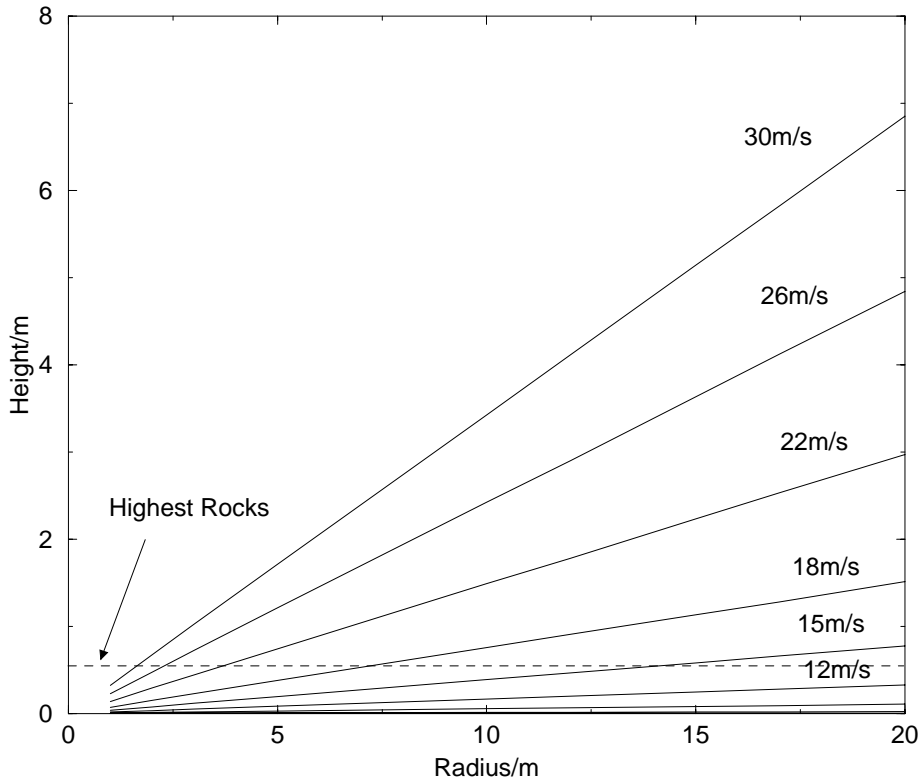


Figure 3.6: Softball maximum step height

3.5.2 Mean free path

In [Wil97], B. Wilcox et alii discuss the implications of Martian rock frequency distributions on the design of wheeled rovers. In particular, they use data from the Viking mission landing sites to calculate the mean free path of a rover; it is defined as the mean distance the rover can go in one direction without encountering a rock too big to climb over.

According to [Wil97], the mean free path may be calculated with the formula

$$x = \frac{1 - \frac{W}{2} \int_{D_0}^{\infty} D\rho(D)dD - \frac{1}{2} \int_{D_0}^{\infty} D^2\rho(D)dD}{W \int_{D_0}^{\infty} \rho(D)dD + \int_{D_0}^{\infty} D\rho(D)dD} \quad (3.13)$$

where $\rho(D)$ is the density of rocks of diameter D , W the robot's width and D_0 the limiting rock diameter, that means the diameter of the greatest rock the Windball can roll over. This value is greater than the maximum step height, because rocks tend to be wider than high.

Table 3.3 gives the values of the integrals needed in (3.13) for Viking landing site 1. Still according to [Wil97], for this site the rocks' heights were about 3/8 their diameters.

We used the data of Viking site 1 and equation (3.13) for our purpose by the following algorithm: A Windball radius and some wind speed are fixed. The maximum step height is calculated by (3.12). This height is multiplied by 8/3 to obtain the corresponding limiting rock diameter.

Table 3.4 shows the results obtained for the Hardball. Figure 3.7 shows a graph of the same data.

D_0	fract. area covered by rocks $> D_0$	$\rho(D_0)$	$\int_{D_0}^{\infty} \rho(D)dD$	$\int_{D_0}^{\infty} D\rho(D)dD$	$\int_{D_0}^{\infty} D^2\rho(D)dD$
0.9000	0.0033	0.0052	0.0052	0.00467	0.0042
0.8400	0.0033	0.0000	0.0052	0.00467	0.0084
0.7600	0.0033	0.0000	0.0052	0.00467	0.0084
0.7200	0.0033	0.0000	0.0052	0.00467	0.0084
0.6700	0.0033	0.0000	0.0052	0.00467	0.0084
0.6300	0.0033	0.0000	0.0052	0.00467	0.0084
0.5600	0.0033	0.0000	0.0052	0.00467	0.0084
0.5300	0.0033	0.0000	0.0052	0.00467	0.0084
0.5200	0.0084	0.0240	0.0292	0.01716	0.0084
0.5000	0.0084	0.0000	0.0292	0.01716	0.0149
0.4800	0.0084	0.0000	0.0292	0.01716	0.0149
0.4700	0.0084	0.0000	0.0292	0.01716	0.0149
0.4600	0.0108	0.0144	0.0436	0.02380	0.0149
0.4500	0.0108	0.0000	0.0436	0.02380	0.0180
0.4300	0.0129	0.0145	0.0581	0.03002	0.0179
0.4200	0.0148	0.0137	0.0718	0.03578	0.0206
0.4100	0.0148	0.0000	0.0718	0.03578	0.0230
0.4000	0.0167	0.0151	0.0869	0.04183	0.0230
0.3800	0.0183	0.0141	0.1010	0.04719	0.0254
0.3700	0.0183	0.0000	0.1010	0.04719	0.0275
0.3600	0.0213	0.0295	0.1305	0.05780	0.0275
0.3500	0.0225	0.0125	0.1430	0.06216	0.0313
0.3300	0.0225	0.0000	0.1430	0.06216	0.0329
0.3200	0.0225	0.0000	0.1430	0.06216	0.0329
0.3100	0.0225	0.0000	0.1430	0.06216	0.0329
0.3000	0.0235	0.0141	0.1571	0.06641	0.0328
0.2900	0.0254	0.0288	0.1859	0.07475	0.0341
0.2800	0.0263	0.0146	0.2005	0.07884	0.0365
0.2700	0.0288	0.0437	0.2441	0.09063	0.0377
0.2600	0.0305	0.0320	0.2762	0.09896	0.0409
0.2500	0.0327	0.0448	0.3210	0.11016	0.0430
0.2400	0.0333	0.0133	0.3343	0.11334	0.0458
0.2300	0.0339	0.0144	0.3487	0.11666	0.0466
0.2200	0.0351	0.0316	0.3803	0.12361	0.0474
0.2100	0.0382	0.0895	0.4698	0.14240	0.0489
0.2000	0.0408	0.0828	0.5526	0.15896	0.0528
0.1900	0.0413	0.0176	0.5702	0.16231	0.0562
0.1800	0.0439	0.1022	0.6724	0.18070	0.0568
0.1700	0.0479	0.1762	0.8486	0.21066	0.0600
0.1600	0.0515	0.1790	1.0276	0.23931	0.0652
0.1500	0.0541	0.1471	1.1748	0.26137	0.0698
0.1400	0.0550	0.0585	1.2332	0.26956	0.0731
0.1300	0.0556	0.0452	1.2784	0.27544	0.0742
0.1200	0.0577	0.1857	1.4641	0.29772	0.0750
0.1100	0.0596	0.1999	1.6641	0.31971	0.0770
0.1000	0.0611	0.1910	1.8550	0.33881	0.0800
0.0900	0.0627	0.2515	2.1065	0.36144	0.0820
0.0800	0.0643	0.3183	2.4249	0.38691	0.0840
0.0700	0.0657	0.3638	2.7886	0.41237	0.0861
0.0600	0.0678	0.7427	3.5314	0.45694	0.0878
0.0500	0.0689	0.5602	4.0916	0.48495	0.0900
0.0400	0.0698	0.7162	4.8078	0.51360	0.0920
0.0300	0.0700	0.2829	5.0907	0.52208	0.0930

Table 3.3: Rock size distribution on Viking landing site 1

mass /kg	radius /m	wind speed / $\frac{m}{s}$									
		3	6	9	12	15	18	22	26	30	
0.127	0.15	—	—	—	—	—	0.45	0.72	1.12	1.70	
0.164	0.2	—	—	—	—	0.35	0.65	1.25	3.45	6.07	
0.316	0.3	—	—	—	0.24	0.52	1.05	4.02	9.03	19.72	
1.10	0.5	—	—	—	0.13	0.36	1.26	4.65	21.23	100.67	
4.20	0.8	—	—	—	0.06	0.15	0.41	3.21	15.37	76.38	
8.10	1	—	—	—	—	0.09	0.25	1.88	12.91	65.77	
13.9	1.2	—	—	—	—	0.05	0.16	0.96	5.64	57.74	
27.1	1.5	—	—	—	—	0.01	0.06	0.49	2.62	48.78	
64.1	2	—	—	—	—	0.00	0.01	0.11	1.22	7.15	

Table 3.4: Hardball mean free path

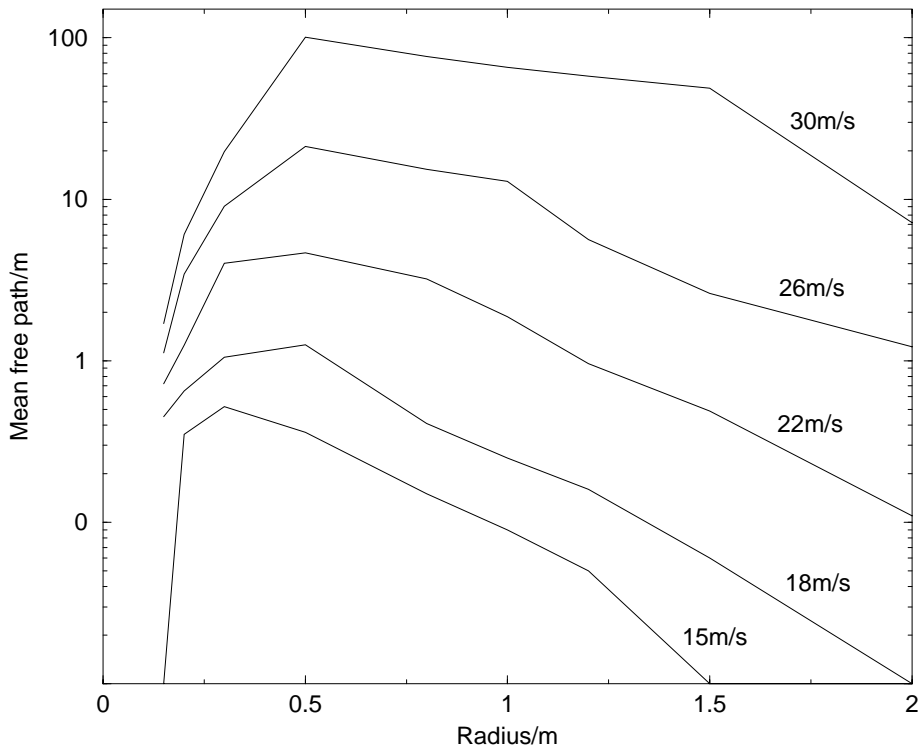


Figure 3.7: Hardball mean free path

For the Softball, (3.13) does not give any reasonable data; for example, for long mean free paths, a saturation can be observed. This is a fault of the model: For limiting rock sizes greater or equal to the biggest rocks that are listed in the statistic, (3.13) does not give diverging mean free path lengths.

The reason for this is that Wilcox's model is based on the implicit assumption that the robot is of roughly the same size as the obstacles. However, with typical Softball sizes greater than several meters, this condition is no longer satisfied.

3.5.3 Model limits

Both layers of the model, the maximum step height as well as the mean free path, include many simplifying assumptions that reduce the reliability of the results:

Maximum step height

The main simplification is the treatment of the flow as being uniform. As pointed out in 2.2.4, the flow near the ground will have a vertical speed gradient and is likely to be turbulent due to the surface's irregular form. The real force acting on the Windball may differ from the one calculated; a non-uniform flow may even create an upward force.

Secondly, the model is purely static. It does not consider fluctuations in the wind speed, which may be in our favour: depending on its strength and duration, a gust could make the Windball climb over a rock that would be considered too high by our model. Plus, we consider the worst case by assuming that the robot has come to rest right in front of a rock - with some momentum it would be a lot easier.

Last but not least the masses used for the two Windball variants are no more than reasonable guesses.

Mean free path

The mean free path model does not really give an idea of how far the robot can go with the wind blowing in one direction. The model allows neither rolling around a rock nor bouncing from the top of one boulder to the next. The distances obtained may be considered greatly underestimated.

The choice of the site - that is, the site of Viking lander 1 - is, obviously, arbitrary. However, according to Wilcox et alii [Wil97], the average rock density seems to be rather lower than higher.

Of course, potential problems like getting stuck in the sand or between two rocks or even falling into a crater or canal were completely neglected.

3.5.4 Model evaluation

Bearing in mind all the restrictions presented in 3.5.3, the results obtained still offer some interesting clues. While the data may not be enough to decide if the *average* wind on Mars is enough or not to move a Windball, it enables us to compare the two variants and estimate their optimal sizes.

For the Hardball, an optimal radius seems to be around 30-50cm (see figure 3.7). For the Softball, the rule is the-bigger-the-better (see figure 3.6); this is plausible if we remember that weight and wind force grow with the square of the robot's dimension, but the relative obstacles' size decreases for growing robot sizes.

Generally, the Softball performs better, but our assumptions on the minimal skin thickness of the Softball must be verified; if we have to use 0.5mm of Kevlar instead of 0.1mm, the Hardball outperforms a Softball of 5m radius by far (figure 3.8).

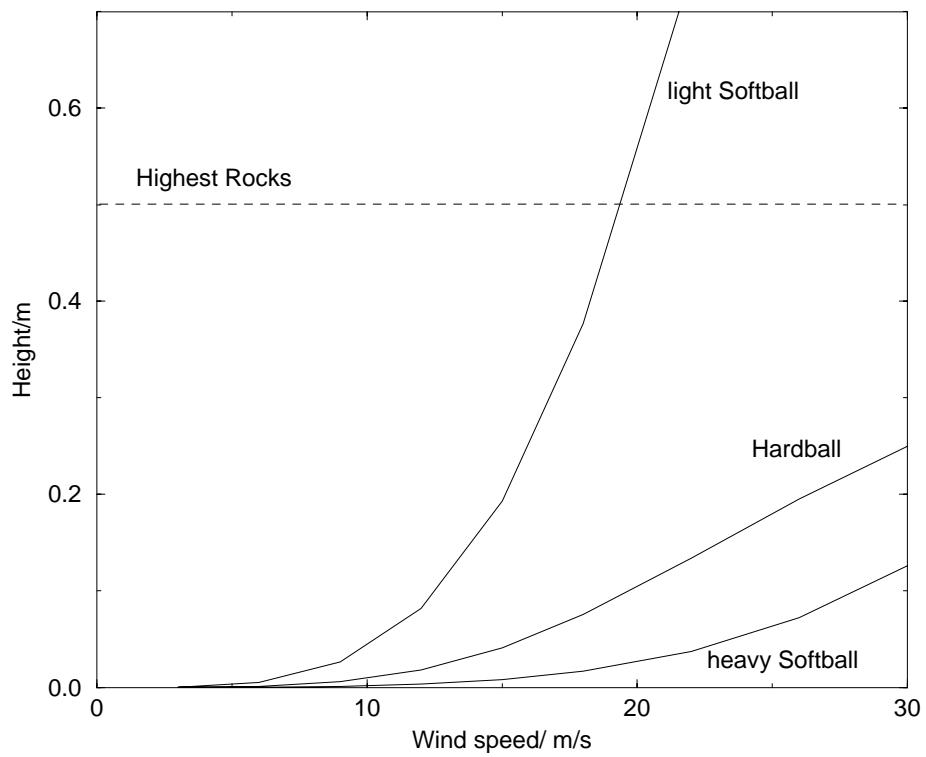


Figure 3.8: Comparison of the Maximum Step Height of a Hardball ($R = 0.5\text{m}$), a light Softball ($R = 5\text{m}$, 0.1mm skin) and a heavier Softball (same radius, but 0.5mm skin)

Chapter 4

Experiments

4.1 Motivation

All in all, the data obtained from the model described in chapter 3 is not satisfactory. The most obvious consequence would be to refine the models used, but eliminating the restraints named in 3.5.3 would be or very costly or even impossible.

So, a different approach is necessary; numerical or breadboard simulation could be possible ways. However, while numerical methods may appear elegant, their application to fluid dynamics is, if it is not restricted to simple cases, a very complex problem. The simulation on a computer of the Windball in a non-uniform flow with obstacles all about would require much more time than was scheduled for the whole Windball project.

Thus, we focused on breadboard simulation. At the civil engineering institute of the EPFL, we found a wind channel installation that was suitable to conduct down-scaled experiments simulating the Windball rolling around on Mars.

4.2 Aims

The general goal of the experiments is to answer the ever-same two questions: Is the wind strong enough to move the robot around in a rocky Martian landscape; and which design parameters yield the best mobility performance?

Before writing this report, only one experiment session could be conducted. So, the short-term goal for these first tries was more modest: Get acquainted with the wind channel installation, see if it is suitable for our purposes and execute simple sample experiments to compare them to our model of chapter 3.

4.3 Setup

In figure 4.1 we can see the main components of our experimental setup: the wind channel itself (about 1m high, 2 meters wide and 10m long), the miniature Windball (diameter 15cm, weight 25.5g, made of foam plastic) marked (A), a step-like obstacle (B) and a hot-wire anemometer to measure the wind speed

